KEK Preprint 94-9
April 1994
A

Cathode-follower RF System for High-intensity Proton Synchrotrons

Y. IRIE, N. KANEKO, Y. KOBAYASHI and Y. YANO

To be published in Nucl. Instrum. Meth., A.

National Laboratory for High Energy Physics, 1994

KEK Reports are available from:

Technical Information & Library
National Laboratory for High Energy Physics
1-1 Oho, Tsukuba-shi
Ibaraki-ken, 305
JAPAN

Phone: 0298-64-1171
Telex: 3652-534 (Domestic)
(0)3652-534 (International)
Fax: 0298-64-4604
Cable: KEK OHO
E-mail: LIBRARY@JPNKEKVX (Bitnet Address)
library@kekvax.kek.jp (Internet Address)

Cathode-follower RF system for high-intensity proton synchrotrons

Y. IRIE, N. KANEKO, Y. KOBAYASHI and Y. YANO

National Laboratory for High Energy Physics, Oho 1-1, Tsukuba, Ibaraki 305, Japan

abstract : A model RF system with a cathode-follower was tested under frequency modulation in the 1-4 MHz range. The repetition rate was 40 Hz. The oscillations were quite stable and no liability to unstable oscillations was observed. An accelerating voltage of 1.2 kV per two cavity-gaps was obtained. An energy problem with the cathode-follower is discussed.

1. Introduction

Beam loading of the RF system is an important subject regarding high-intensity accelerators. Artificial techniques, such as beam-feedforward[1-3] and fast voltage feedback[4] loops, as well as a cathode-follower (CF) RF amplifier[5] have been adopted to reduce the output impedance seen by the beam. A conceptual design was considered in reference 6) upon the CF RF system for high-current beam storage rings. The CF was first implemented as a beam buncher in the Proton Storage Ring at the Los Alamos National Laboratory. However, for further application of the CF to synchrotrons it is necessary to investigate the feasibility under frequency modulation. A model RF system with a 40 KW triode as a final amplifier was tested for this purpose, the frequency range of which was 1-4 MHz and the repetition was 40 Hz.

The theoretical aspects of the CF are discussed in section 2 and the experimental results are given in sections 4 and 5. Since the gain of the CF is less than unity, power consumption in the driver stage is significant. The energy problem in the driver stage is mentioned in section 6.

2. Theoretical aspects

The CF is inherently liable to oscillations when the cathode load is capacitively tuned (fig.1). If the grid current (i_g) is negligible compared to the other branch currents, the cathode voltage (e_k) is given by

$$e_k = \frac{\mu}{\mu + 1} e_{in} \frac{Z_k}{r/(\mu + 1) + Z_k},$$

where μ is the amplification factor, r the plate resistance and the beam is assumed to be absent for the moment. Z_k is the cathode load which comprises a parallel resonant circuit and is given by

$$Z_k = \frac{1}{C} \frac{s}{s^2 + s/CR + \omega_0^2},$$

where R is the shunt resistance and ω_0 the cavity resonant frequency ($1/\sqrt{LC}$). Since $-i_g = j\,\omega\, C_g\,(e_k - e_{in})$, where C_g is the cathode-grid capacitance, the scalar product of e_{in} and $-i_g$ is negative for an inductive load and is positive for a capacitive load, as can be seen from the phasor diagram in fig.2. The energy is then fed back to the driver stage through C_g for the latter case, and the unstable operation can potentially occur for some driver-stage conditions. This instability has been discussed by many authors [7, 8] in terms of negative resistance. However, since the phenomenon is transient, the stability criterion is applied.

Suppose that the driver stage comprises a tank circuit (L_d, C_d), and the cathode load an RF

cavity with beam current (i_b). The driver-stage voltage is then written as

$$e_{in} = -\frac{I_1 s + I_2 \omega}{s^2 + \omega^2} \frac{s^3 C_g L_d r}{a_0 s^4 + a_1 s^3 + a_2 s^2 + a_3 s + a_4}, \tag{1}$$

where $i_b = (I_1 s + I_2 \omega)/(s^2 + \omega^2)$ and the coefficients in the denominator are:

$$\begin{aligned} a_0 &= (C_d C_g + C_g C + C C_d) L_d r, \\ a_1 &= C_g L_d + (\mu + 1) C_d L_d + (C_d + C_g) L_d r / R, \\ a_2 &= \left[C + C_g + \omega_0^2 C (C_d + C_g) L_d\right] r, \\ a_3 &= \mu + 1 + r / R \end{aligned} \tag{2}$$

and

$$a_4 = \omega_0^2 C r.$$

It is interesting that no beam component appears in these coefficients, ie beam loading has no influence upon the stability criterion. The following terms should have a positive sign for stable operation:

$$b_1 = (a_1 a_2 - a_0 a_3)/a_1 \text{ and } c_1 = (a_3 b_1 - a_1 a_4)/b_1, \tag{3}$$

where the other terms which are definitely positive are not shown. Assuming that C_g is small compared to C and C_d, these are approximated by

$$b_1 \approx \omega_0^2 C C_d L_d r > 0$$

and

$$c_1 \approx \frac{\mu C_g \left(\omega_0^2 C_d L_d - 1\right)}{\omega_0^2 C_d^2 L_d}. \tag{4}$$

The c_1 changes sign when the resonant frequency of the driver circuit differs from that of the cathode load. For a capacitive load, it is negative and the system becomes unstable, which is consistent with the discussion given above. The exact form of eq. (3) is given in the appendix. In the unstable case, it is effective to install a resistor in series with the cathode-grid capacitance for stabilization or for slowing the divergence. The polynomial in the denominator, as in eq. (1), is then fifth order in s and the expressions of the stability criterion become rather complicated. Therefore, only the numerical results are presented to ascertain the role of the series resistor (ρ). Fig. 3 shows the term which changes sign for the variable range considered; the other terms are all positive. It is seen that cavity tuning is also essential for stability. In the case when $\omega_0^2 C_d L_d = 0.98$, the time constants of the divergence are 0.63, 0.64 and 2.5 msec for ρ=0, 30 and 1500 ohms, respectively.

Another aspect of the CF is due to the low output impedance, $r/(\mu+1)$. As for the cathode current (i_k), it easily distorts if only a small amount of harmonics is mixed in the grid input voltage. For higher harmonics, the load (Z_k) is almost shorted with the cavity capacitance (C) and $r/(\mu+1)$ remains as the load, while $r/(\mu+1)$ in series with R is the load for the fundamental component. Since R is usually much higher than $r/(\mu+1)$, the harmonic components in the cathode current are enhanced. A comparison with experiments is given in section 5. As for the voltages, the phase difference between the driver-stage and cavity voltages is less sensitive to the cavity tuning. Hence, it is not precise to tune the cavity in the conventional way, ie by a phase comparison of the two voltages.

3. RF system

Fig. 4 shows the system setup. Two cavities are connected by a single-turn bias winding, either of which is directly coupled to the cathode of the final amplifier. The Eimac triode (3CW40,000H3) is used as the CF. Five ferrite rings with cooling plates are stacked in each cavity. A 30-ohm resistor is installed at the grid input to prevent the likelihood of unstable oscillations; a case without the resistor was also tested. In the driver stage a high-power tetrode (max. plate dissipation 90 KW) drives a 500-ohm resistor across the grid input. The inductance at the plate circuit is high enough to keep the resonant frequency of the driver stage lower than 1 MHz. The bias power supply for cavity ferrites comprises a dc plus a resonant power supply. The output current has the shape of the dc-biased sinusoidal wave at a 40 Hz repetition. Since the ac amplitude was limited to 250 A, the bias current was divided into three groups (200-700 A, 700-1200 A and 1200-1700 A) to cover the entire range of the RF frequency of interest. Table 1 summarises the parameters.

Fig. 5 shows the shunt impedance and resonant frequency of the cavities at each dc bias current, measured by a Hewlett Packard 4195A network/spectrum analyser. Although the impedance curve had a dip near to 300 A, the reason was not investigated further since the cavity gap was shorted by the low output impedance of the CF and the dip did not alter the following results.

A Tektronix programmable arbitrary/function generator (AFG5101) produces a reference voltage with 12-bit resolution for a voltage-controlled oscillator (VCO). The full scale of the memory is 8192 points. The reference waveform is created on an IBM personal computer (model 70386) by referring to the curve in fig. 5, which is roughly consistent with the ac bias current at 40 Hz. The waveform can be edited during the course of RF excitation to reduce the phase difference between the grid and cathode voltage; after the excitation reaches an acceptable level for the phase detector, the phase feedback loop is enabled. The software is a WaveWriter package which runs in a Microsoft Windows environment. The start of the generator cycle is synchronized with the repetition of the bias power supply. A Pearson model 150 current transformer is used to monitor the cathode current. The level control loop is incorporated only to keep the preamplifier output constant.

4. Output impedance

In measuring the output impedance of the system, the probe of the 4195A was connected to the 'cold' gap of the cavity where no quiescent current flows. Fig. 6 shows a typical result compared with calculations using an electronic circuit simulation program, Spice. In the calculation $\mu = 18$, $r = 370$ ohms, $C_g = 70$ pF and any stray capacitances across the grid input were estimated to be 123 pF. The bias current for ferrites was adjusted to the resonance at 2.4 MHz. The peak at 4.3 MHz showed a parasitic resonance through the inductance (0.36 μH) of the bias winding loop, where the gap voltages of the two cavities swung 180° out-of-phase with nearly the same amplitudes.[9] The calculation also fits the other spikes and the steep slope at higher frequencies, where contributions are from the lead inductance of the measuring probe and the cavity capacitors, as well as the bypass capacitor at the feeding point of the cavity bias current.

The output impedance seen by the beam is summarised in fig. 7. During the measurements, the parasitic peak always located at the higher frequency side of the main resonance point, and they did not overlap. In the figure, a slight increase in the impedance with frequency is due to the fact that the voltage between the cathode and grid becomes less sensitive to the cavity voltage with increasing frequency because of $1/\omega C_g$ [8]; hence, the characteristic of low output impedance is diminished. To make the calculation independent of the cavities, we directly look into the cathode and the cathode-grid reactance in series with whatever appears between the grid and ground in the driver stage. The impedance thus seen gives $r/(\mu+1)$ at a lower frequency, and

increases with frequency. The results for the present system are 19 ohms$\angle 4°$ at 500 kHz and 29 ohms$\angle$-13° at 50 MHz.

The similar resonances with fig. 6 were obtained by a Spice calculation for the grid input impedance. In fig. 8, the dashed line approximates the impedance seen by the driver amplifier, where the cathode impedance is set to be the shunt resistance, which is validated if the cavity is continually kept at resonance throughout the repetition cycle. The broad resonance peaking around 0.9 MHz shows that the driver stage comprises a tank circuit which includes an inductor in the plate circuit of the driver amplifier. At higher frequencies the impedance decreases inversely with the frequency.

5. High power results

The experiments were carried out over three frequency ranges, ie 1.0-2.6, 2.2-3.2 and 3.0-3.8 MHz, according to the three groups of bias currents. The anode voltage and quiescent current of the CF were 5 KV and 6.5 A, respectively. Figs. 9 and 10 show typical RF envelopes and the detailed waveforms, respectively. Although the current waveforms were distorted significantly, the oscillations were quite stable and no liability to unstable oscillations was observed; 1.2 KV was obtained for the peak RF voltage per two gaps. A scheme without a 30-ohm damping resistor was also examined so as to see whether an instability occurs; however, contrary to our concern, the result showed no unstable oscillations.

The frequency spectrum was analysed by using the 4195A for the driver-stage voltage and cathode current at 1.1 MHz under a dc bias current. The waveform was very similar to the photo at 1.19 MHz in fig. 10. The results are shown in table 2, where the enhancement is compared with a simple calculation. According to the discussion in section 2, the enhancement is defined as the ratio of the relative component of current to that of voltage and is given by

$$\left(\frac{r}{\mu+1}+R\right)\Big/\left|\frac{r}{\mu+1}+\frac{1}{j\omega C}\right|, \tag{5}$$

where C is 5.25 nF and R is 120 ohms, which is derived from the fundamental components of the voltage and current. The general trend is well explained by the simple model.

The behavior around the cavity resonant frequency was studied whether an instability with a longer time constant occurs. The test was performed at various current levels of dc biasing, where the VCO frequency was slightly shifted from the resonance point. However, the present CF system also showed stable operation. This is because no relevant tank circuit exists in the driver stage, as discussed in section 2.

6. Discussions

As was shown in fig. 8, the capacitance across the grid input is dominant at higher frequencies and the power necessary for driving the CF becomes intolerable, since the voltage gain is less than unity. A resonating tank circuit in the driver stage may be thought to circumvent the power consumption. However, such a scheme requires another set of bias power supplies for tuning, which makes the RF system complicated. It is also difficult to precisely tune both of these tank circuits because of the interference through the cathode-grid capacitance[9]. From an output impedance point of view, such a high-impedance scheme is not appropriate since it diminishes the low-impedance characteristics. A peaking method may be available to extend the bandwidth. Except for these difficulties, the CF provides only a few ohms as an output impedance, depending upon the choice of the vacuum tube. Ref. 5 shows the $r/(\mu+1)$ to be 3 ohms by using an Amperex 8918, the plate dissipation of which is 300 KW.

The waveform distortion of the driver-stage voltage is mainly due to a faulty aspect of the preamplifier itself in figure 4, because the output is not purely sinusoidal and is distorted near to 1 MHz. The improvement of the preamplifier to realize a wideband characteristics will help

present more sine-like waveforms in the cathode voltage and current, which enables a better tuning of the cavity by comparing these two phases.

7. Conclusion

A model RF system with a cathode-follower was tested under frequency modulation in the 1-4 MHz range. The repetition rate was 40 Hz. Contrary to our concern for an inherent instability of the cathode-follower, the oscillation has proved to be quite stable. Although the improvement in the preamplifier characteristics is necessary for any further feasibility study, the cathode-follower is expected to be applicable for heavy beam-loading synchrotrons at low-frequency ranges where the grid input impedance is relatively high.

Appendix : The exact form of eq. (3) is expressed as

$$b_1 = r\,\frac{\left\{\begin{array}{c}(\mu+1)\left[C\,C_g\left(\omega_0^2\,C_d\,L_d - 1\right) + \omega_0^2\,C_d^2\,L_d\,C\right] + C_g\left[C + C_g + \omega_0^2\,C\,(C_d + C_g)\,L_d\right] \\ + \left[C_g^2 + \omega_0^2\,C\,(C_d + C_g)^2\,L_d\right] r/R\end{array}\right\}}{C_g + (\mu+1)\,C_d + (C_d + C_g)\,r/R},$$

and

$$c_1 = C_g\,\frac{\left\{\begin{array}{c}(\mu+1)^2\,C\,\left(\omega_0^2\,C_d\,L_d - 1\right) \\ + (\mu+1)\left\{C + C_g - (C - C_g)\,r/R + \omega_0^2\,C\,\left[(C_d + C_g)\,L_d\,r/R - (C_d - C_g)\,L_d\right]\right\} \\ + C_g\,(r/R)^2 + (C + C_g)\,r/R - \omega_0^2\,C\,L_d\left[C_g + (C_d + C_g)\,r/R\right]\end{array}\right\}}{\left\{\begin{array}{c}(\mu+1)\left[C\,C_g\left(\omega_0^2\,C_d\,L_d - 1\right) + \omega_0^2\,C_d^2\,L_d\,C\right] + C_g\left[C + C_g + \omega_0^2\,C\,(C_d + C_g)\,L_d\right] \\ + \left[C_g^2 + \omega_0^2\,C\,(C_d + C_g)^2\,L_d\right] r/R\end{array}\right\}}.$$

References:

1) H. Frischholz and W. Schnell: IEEE Trans. Nucl. Sci. Vol. NS-24, No. 3, June 1977, pp. 1683-1685.

2) G. H. Rees: IEEE Trans. Nucl. Sci. Vol. NS-28, No. 3, June 1981, pp. 2125-2127.

3) E. Raka et al: IEEE Trans. Nucl. Sci. Vol. NS-32, No. 5, October 1985, pp. 3110-3112.

4) J. Baillod et al: IEEE Trans. Nucl. Sci. Vol. NS-30, No. 4, August 1983, pp. 3499-3501.

5) T. Hardek: IEEE Conference Record, Power Modulator Symposium, Arlington, Virginia, June 1984, pp. 207-211.

6) A. Luccio and M. Puglisi: Particle Accelerators, Vol. 11, 1981, pp.153-160.

7) K. Schlesinger: Proc. I.R.E., Vol. 33, December 1945, pp.843-855.

8) F. Clapp: Proc. I.R.E., Vol. 37, August 1949, pp.932-937.

9) Y. Irie et al: KEK Report 87-28, National Laboratory for High Energy Physics, February 1988.

Table 1. Parameters of the cathode-follower RF system

Repetition frequency		40	Hz
RF frequency		1~4	MHz
Cavity			
Inductance		2.4~0.15	μH
Resonating capacitance		10.5	nF
Ferrite	material	Ni-Zn	
	inner radius	0.12	m
	outer radius	0.22	m
	thickness	0.025	m
No. of ferrite rings / cavity		5	
Bias loop		1	turn
Bias current		200~1700	ampere
Final Amplifier			
Class of operation		A	
Type		cathode-follower	
Configuration		single-ended	
Power tube		Eimac 3CW40,000H3	
Driver Amplifier			
Class of operation		A	
Type		grounded cathode	
Power tube		Ziemens RS2058CJ	

Table 2. Waveform distortion. The voltage and current are relative values to the fundamental components. The calculation uses eq.(5).

harmonic no.	driver-stage voltage	cathode current	enhancement	calculation
2	1.1×10^{-2}	6.7×10^{-2}	6.1	7.0
3	9.6×10^{-2}	6.0×10^{-1}	6.2	7.1

FIGURE CAPTIONS:

Fig. 1 Cathode-follower and its equivalent circuit.

Fig. 2 Phasor diagram of the cathode-follower.

Fig. 3 Stability criterion. The number of each line denotes $\omega_0^2 C_d L_d$. The parameters are: L=1.07 μH, C=10.5 nF, R=200 Ω, C_g=70 pF, r=370 Ω, μ=18, L_d=2 μH and C_d is varied from 5 to 6 nF.

Fig. 4 Setup of the RF system.

Fig. 5 Shunt impedance and resonant frequency of the two cavities coupled by a bias loop. The measurement was performed at each dc current with increasing direction from 0 to 1800 A, and decreasing in reverse. Hysteresis is clearly seen.

Fig. 6 Typical result of an output impedance measurement.

Fig. 7 Output impedance seen by the circulating beam.

Fig. 8 Grid input impedance when the cavity is tuned under the same condition as in fig. 6 (solid line). As for the dashed line, the cathode impedance is taken to be the shunt resistance.

Fig. 9 The RF envelopes in the ranges of (a) 1.0-2.6, (b) 2.2-3.2 and (c) 3.0-3.8 MHz. From the upper to the lower traces: the grid input voltage (500 V/div.), the cathode current (10 A/div.), and the cathode voltage (500 V/div.).

Fig. 10 Detailed waveforms at the frequencies shown in the upper right in the photos. From the upper to the lower traces: the grid input voltage (500 V/div.), the cathode current (4 A/div.), and the cathode voltage (500 V/div.).

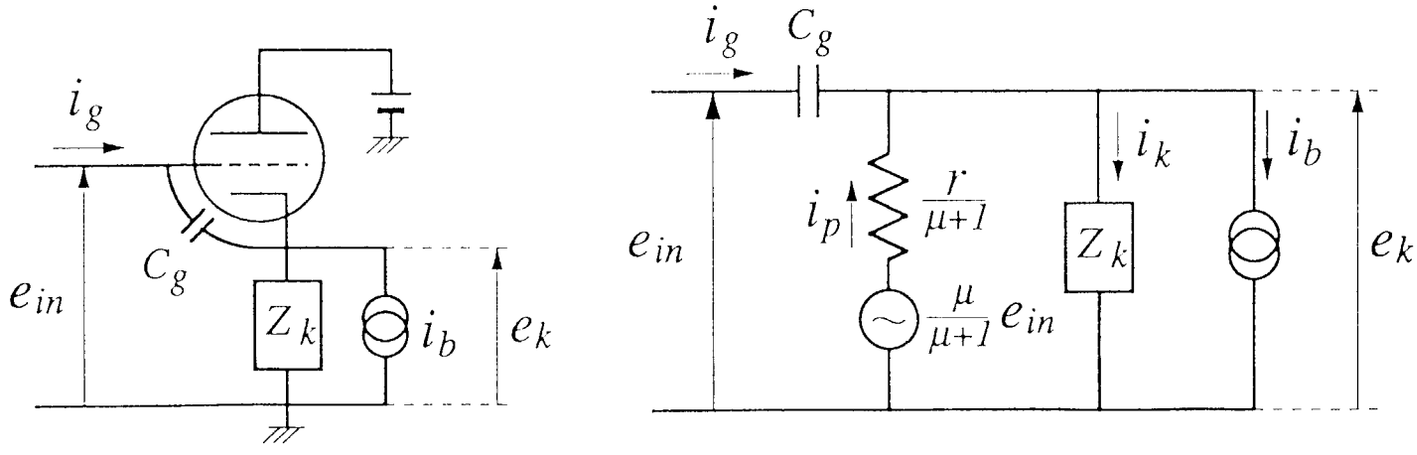
i_g
C_g
e_{in}
Z_k
i_b
e_k
i_g
C_g
i_p
$\frac{r}{\mu+1}$
e_{in}
$\frac{\mu}{\mu+1} e_{in}$
i_k
i_b
Z_k
e_k

Fig. 1

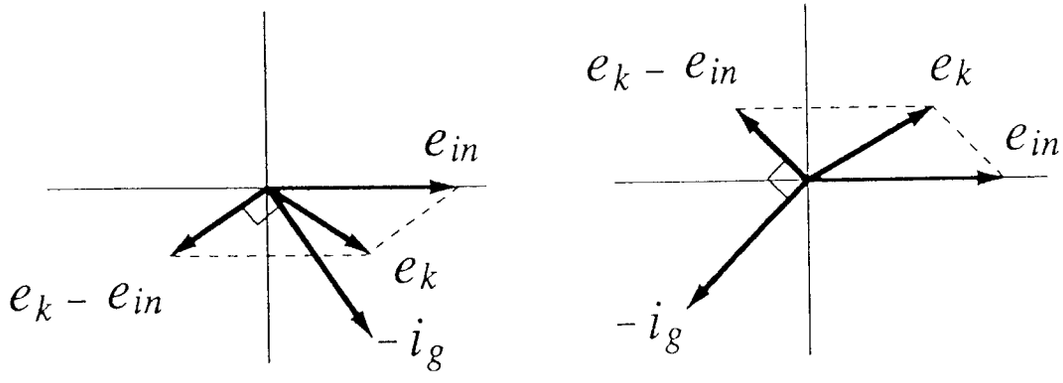

capacitive tuning:
$(e_k \cdot -i_g) > 0$

inductive tuning:
$(e_k \cdot -i_g) < 0$

Fig. 2

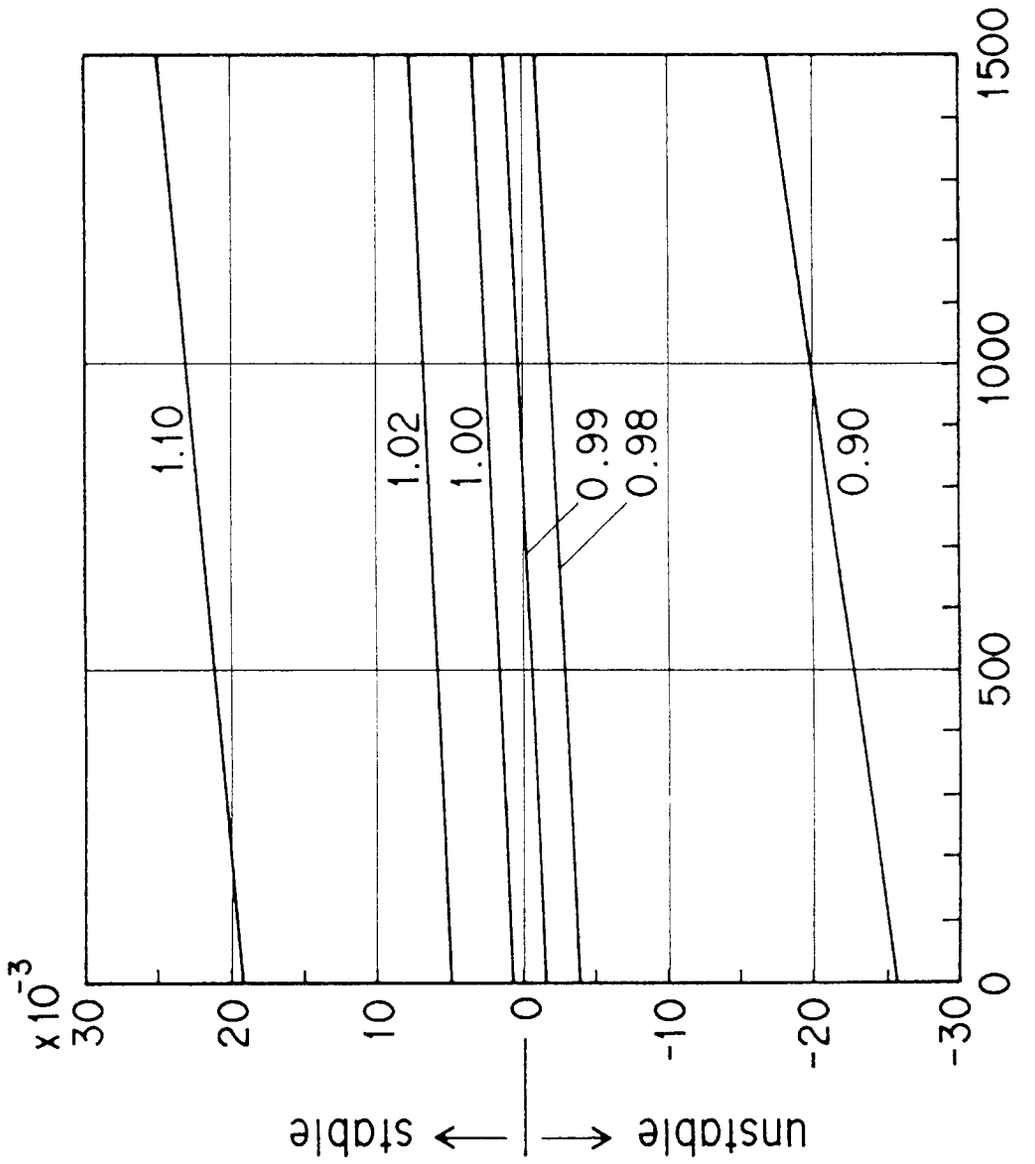
x10^-3
30
20
10
0
-10
-20
-30
stable
unstable
0
500
1000
1500
series resistance [ohm]
1.10
1.02
1.00
0.99
0.98
0.90

Fig. 3

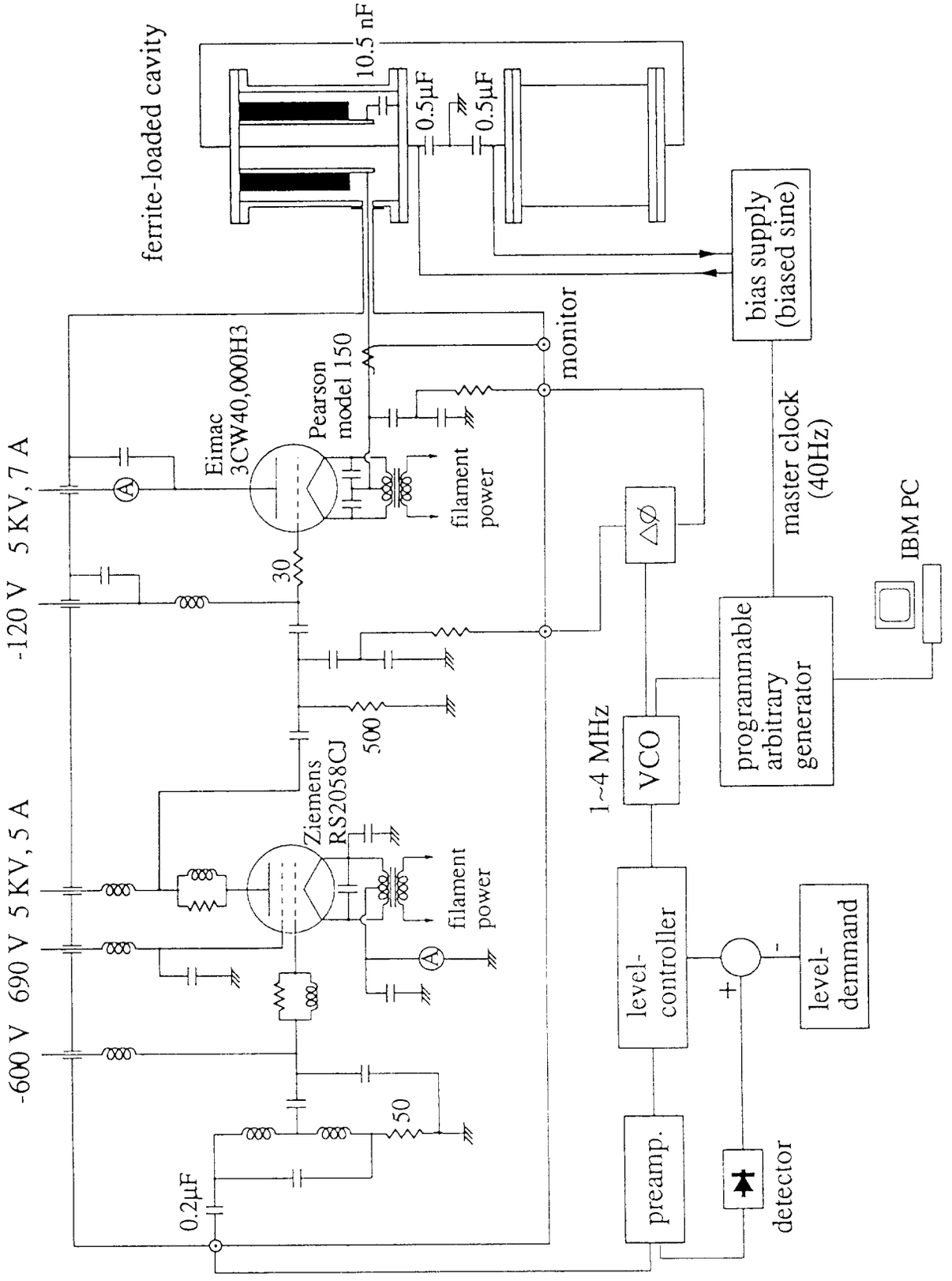
ferrite-loaded cavity
10.5 nF
0.5μF
0.5μF
bias supply
(biased sine)
monitor
Eimac
3CW40,000H3
Pearson
model 150
filament
power
-120 V 5 KV, 7 A
30
master clock
(40Hz)
IBM PC
△Ø
programmable
arbitrary
generator
500
Ziemens
RS2058CJ
1~4 MHz
VCO
filament
power
-600 V 690 V 5 KV, 5 A
level-
controller
level-
demmand
50
0.2μF
preamp.
detector

Fig. 4

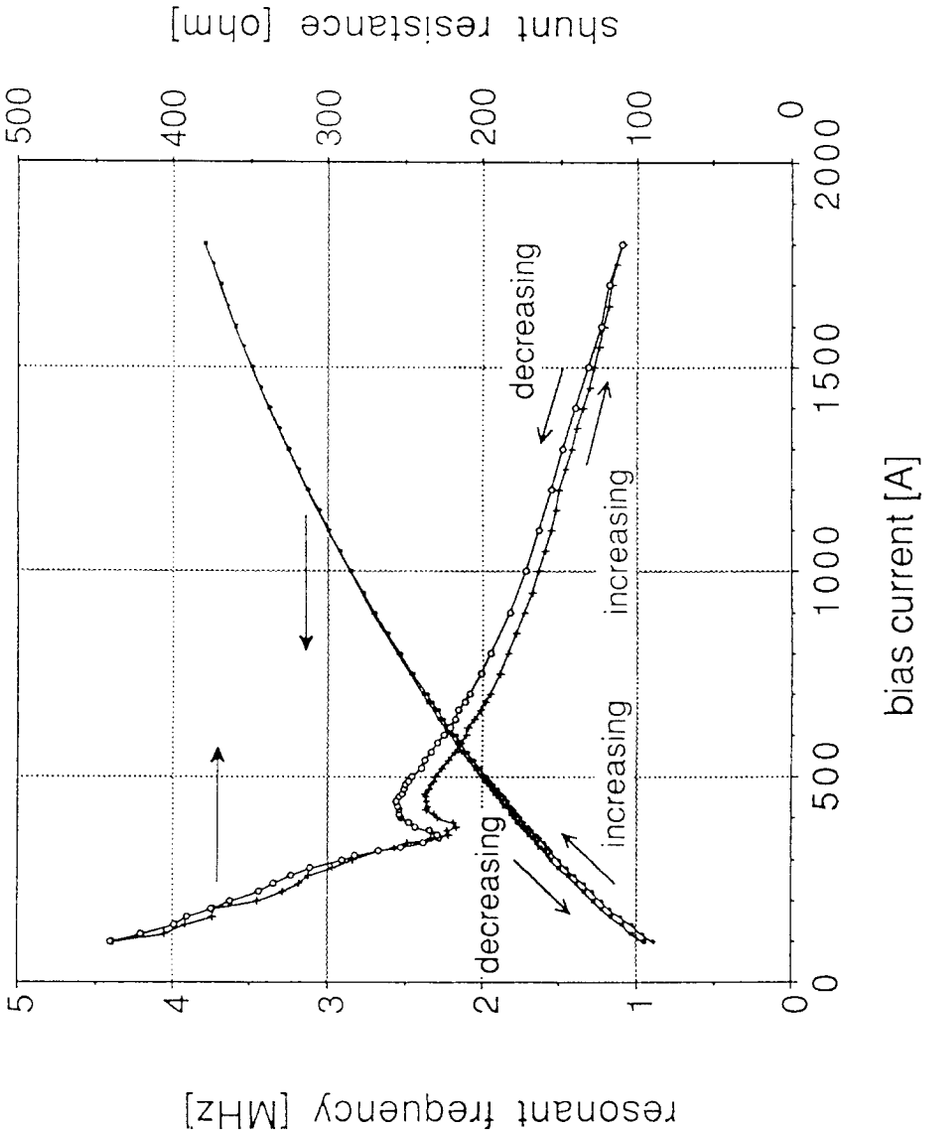
shunt resistance [ohm]
500
400
300
200
100
0
resonant frequency [MHz]
5
4
3
2
1
0
0
500
1000
1500
2000
bias current [A]
decreasing
increasing
increasing
decreasing

Fig. 5

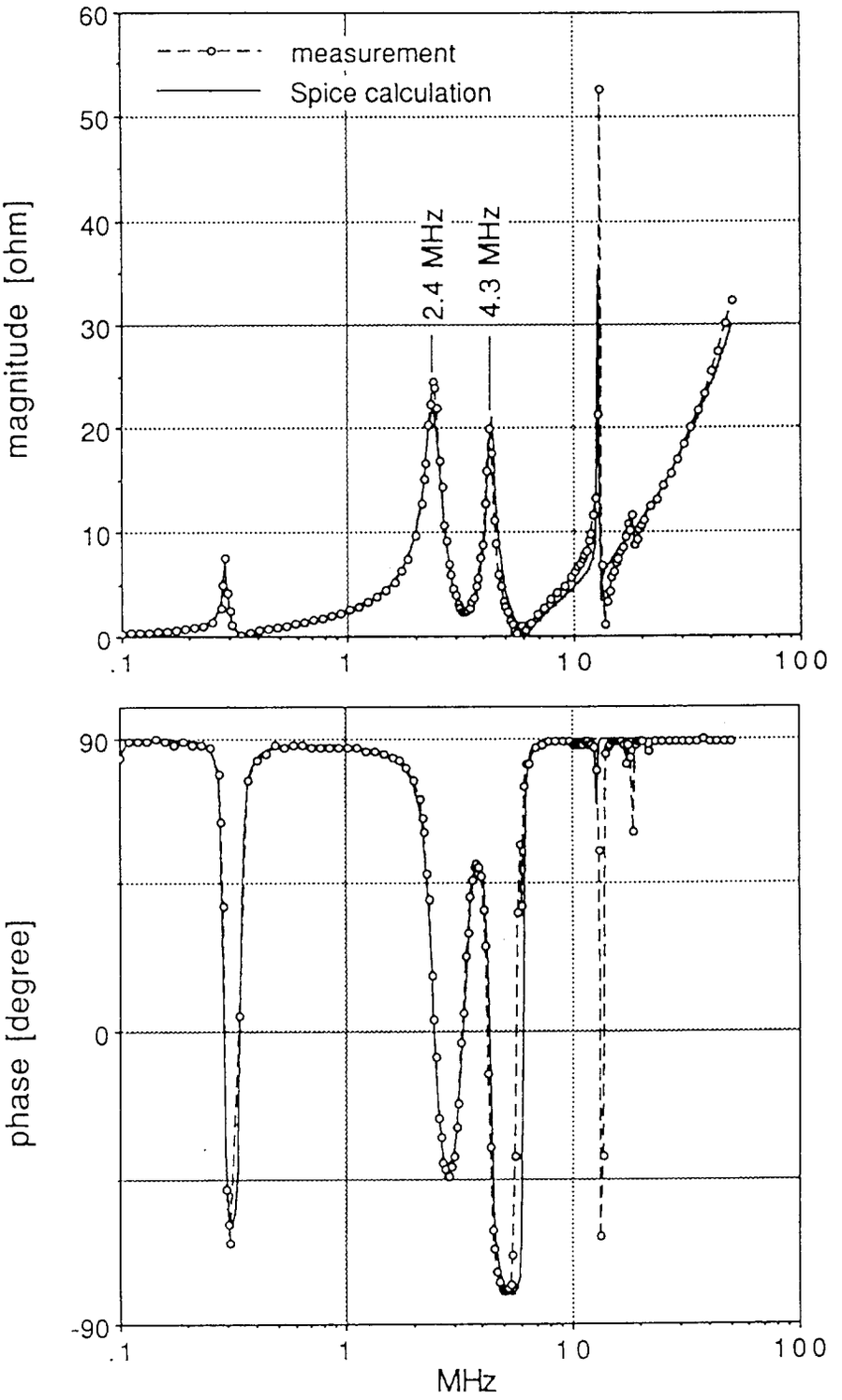
measurement
Spice calculation
2.4 MHz
4.3 MHz
magnitude [ohm]
60
50
40
30
20
10
0
.1
1
10
100
phase [degree]
90
0
-90
MHz

Fig. 6

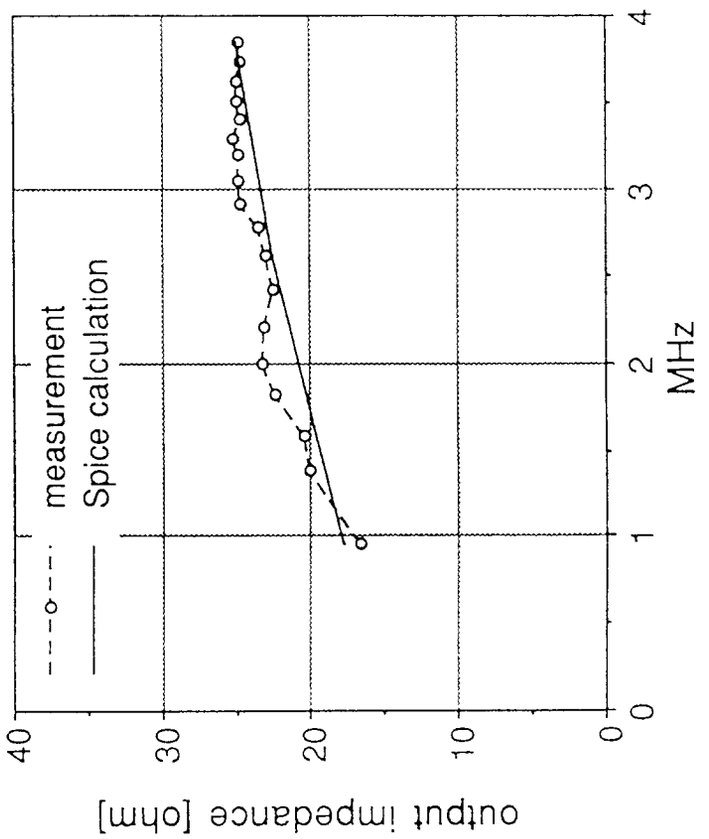
output impedance [ohm]
40
30
20
10
0
0
1
2
3
4
MHz
measurement
Spice calculation

Fig. 7

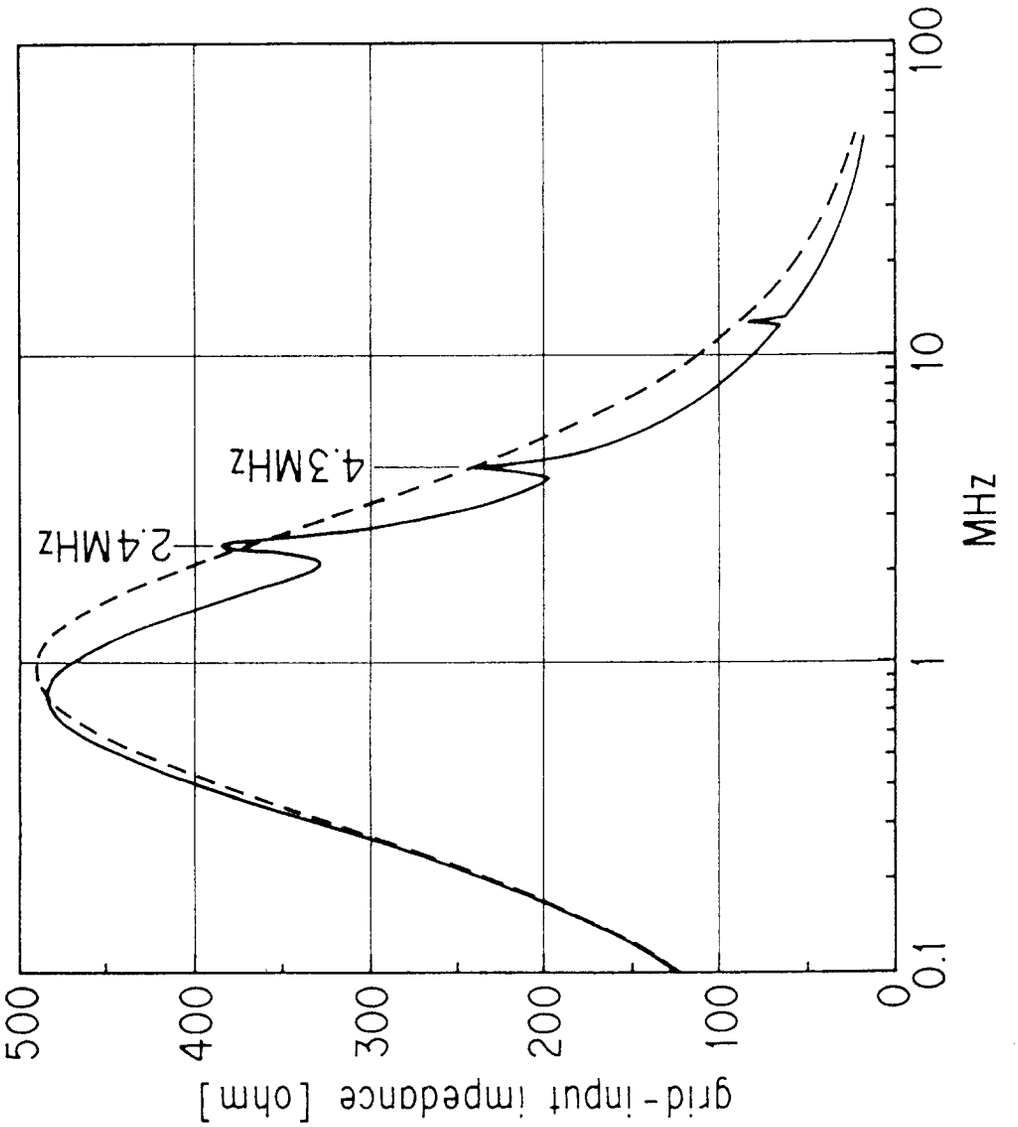
grid-input impedance [ohm]
500
400
300
200
100
0
0.1
1
10
100
MHz
4.3MHz
2.4MHz

Fig. 8

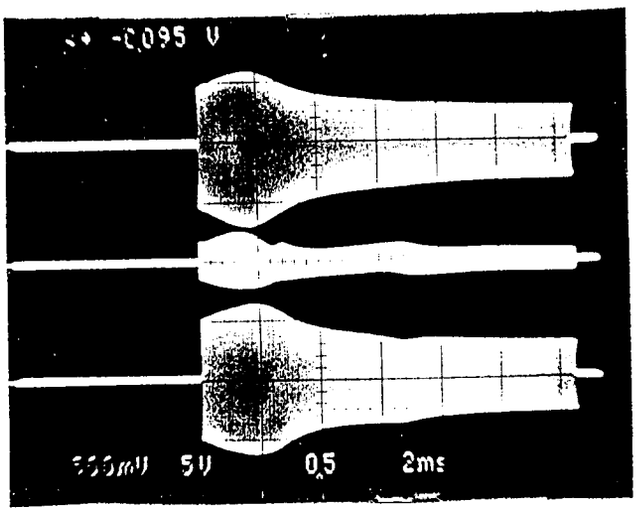

(a)

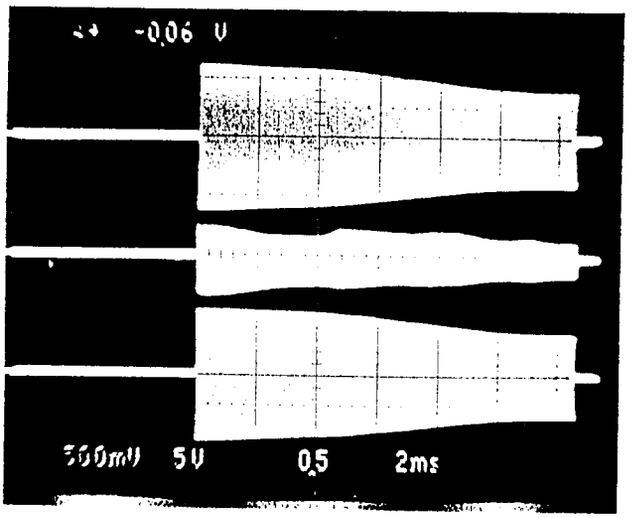

(b)

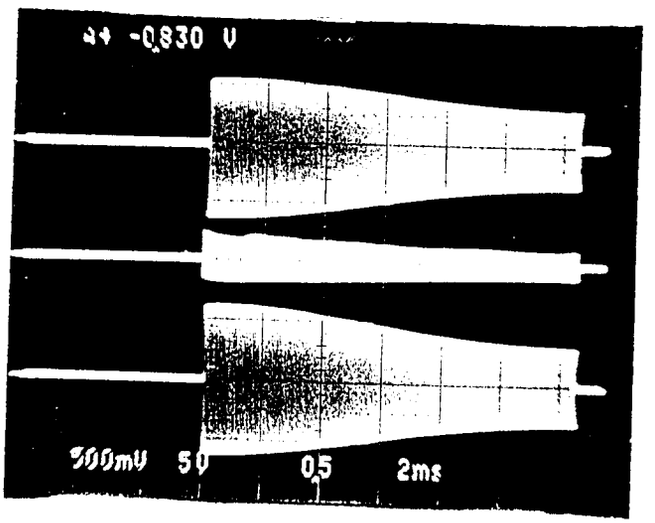

(c)

Fig. 9

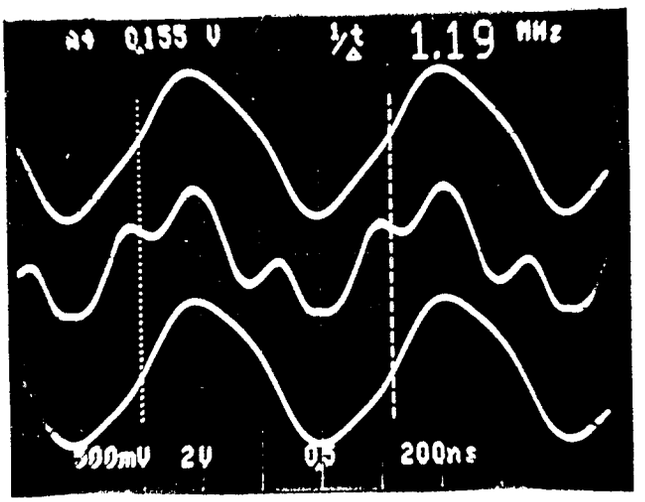
Q155 V
1/Δt 1.19 MHz
500mV 2V 0.5 200ns

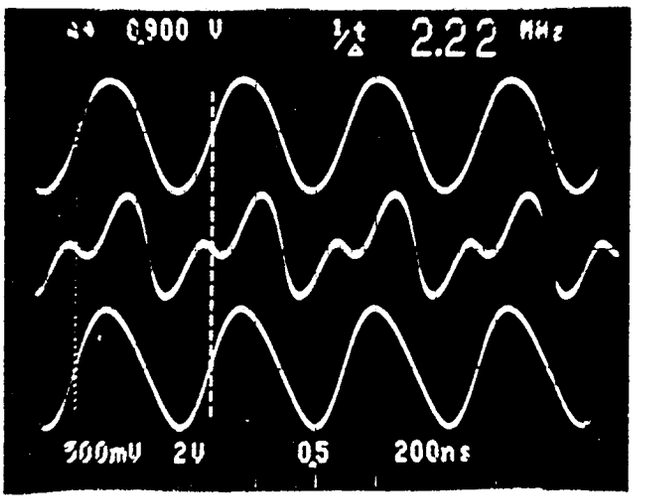
Q900 V
1/Δt 2.22 MHz
500mV 2V 0.5 200ns

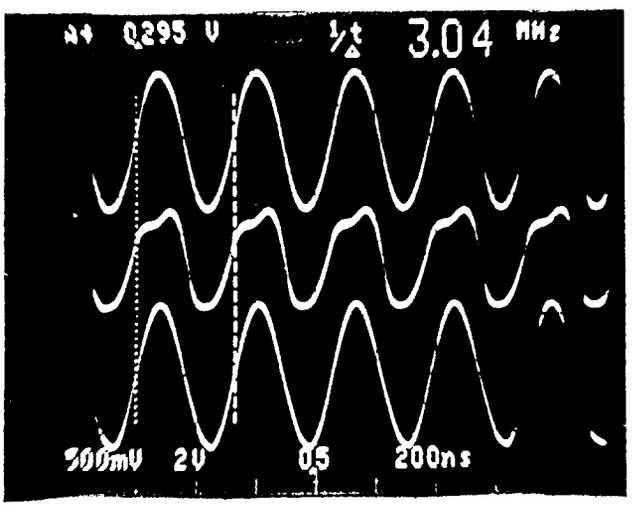
Q295 V
1/Δt 3.04 MHz
500mV 2V 0.5 200ns

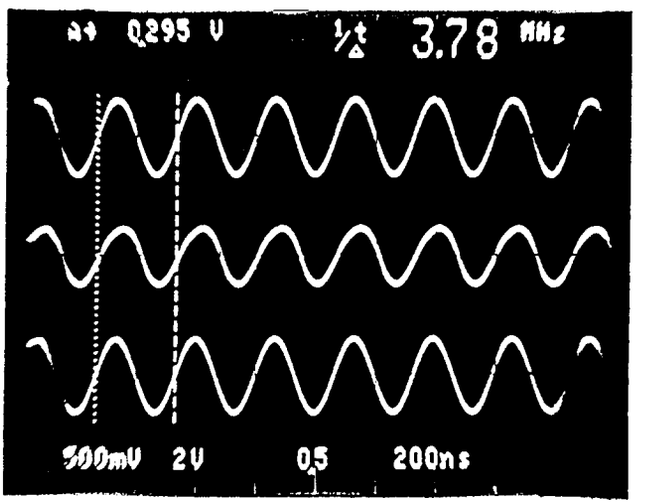
Q295 V
1/Δt 3.78 MHz
500mV 2V 0.5 200ns

Fig. 10